Extreme Multielectron Ionization of Elemental Clusters in Ultraintense Laser Fields

ANDREAS HEIDENREICH, ISIDORE LAST, AND JOSHUA JORTNER*
School of Chemistry, Raymond and Beverly Sackler Faculty of Exact Sciences, Tel Aviv University, Tel Aviv 69978, Israel

(Received 28 September 2006 and in revised form 23 October 2006)

Abstract. In this paper we present computational and theoretical studies of extreme multielectron ionization in Xe_n clusters (n = 55–2171, initial cluster radii R_0 = 8.7–31.0 Å) driven by ultraintense Gaussian infrared laser fields (peak intensity I_M = 10^{15}–10^{20} W cm^{-2}, temporal pulse length τ = 10–100 fs, and frequency ν = 0.35fs^{-1}). The microscopic approach, which rests on three sequential–parallel processes of inner ionization, nanoplasma formation, and outer ionization, properly describes the high ionization levels (with the formation of $\{Xe^{q+}\}_n$ with q = 5–36), the inner/outer cluster ionization mechanisms, and the nanoplasma response. The cluster size and laser intensity dependence of the inner ionization levels are determined by a complex superposition of laser-induced barrier suppression ionization (BSI), with the contributions of the inner field BSI manifesting ignition enhancement and screening retardation effects, together with electron impact ionization. The positively charged nanoplasma produced by inner ionization reveals intensity-dependent spatial inhomogeneity and spatial anisotropy, and can be either persistent (at lower intensities) or transient (at higher intensities). The nanoplasma is depleted by outer ionization that was semiquantitatively described by the cluster barrier suppression electrostatic model, which accounts for the cluster size, laser intensity, and pulse length dependence of the outer ionization yield.

1. PROLOGUE

With the advent of ultraintense lasers[1,2] (peak intensities I_M = 10^{15}–10^{20} W cm^{-2}, temporal widths τ = 10–100 fs), remarkable progress has been made in the exploration of laser–matter interaction. The realm of ultrafast phenomena in molecular science currently moves from femtosecond chemistry on the timescale of nuclear motion[3–6] towards attosecond chemistry of electron dynamics.[7–10] This new attosecond temporal regime for dynamics constitutes a "spin off" of ultraintense laser–matter interactions. In the attosecond domain, nonperturbative effects are fundamental and new mechanisms of ionization and of multielectron dynamics in atoms, molecules, clusters, plasmas, and condensed matter are unveiled. In this context, the response of clusters to ultraintense laser fields drives novel ionization processes[11–40] and manifests new features of electron dynamics.[11,15,16,25,29,32,34,37,40–44]

To circumvent the debris problem[45] from macroscopic solid targets driven by ultraintense lasers, it is imperative to explore efficient laser energy acquisition and disposal in elemental and molecular clusters. These constitute large, finite systems with a density comparable to that of the solid or liquid condensed phase. The cluster response to ultraintense laser fields triggers well-characterized ultrafast electron dynamics (on the timescale of <1–100 fs). The response of clusters to ultraintense laser fields (I = 10^{15}–10^{20} W cm^{-2}) is distinct both from the electron dynamic response in ordinary fields ($I \lesssim 10^{13}$ W cm^{-2}), where perturbative quantum electrodynamics is applicable, and from the response of "small" atoms or molecules to ultraintense laser fields, which is triggered by the barrier suppression single-step

*Author to whom correspondence should be addressed.
E-mail: jortner@chemsg1.tau.ac.il

ionization mechanism. When the cluster size (or the size of a large chemical system) significantly exceeds the size of the constituent barrier distance, a well-characterized compound cluster ionization mechanism is manifested. The compound, extreme multielectron ionization mechanism of clusters involves three sequential–parallel processes of inner ionization, nanoplasma formation, and outer ionization.[13,14,18,19,25,29–31,43] Inner ionization results in the formation of a charged, energetic nanoplasma within the cluster and in its vicinity, which is followed by the partial or complete outer ionization of the nanoplasma.[11,21,29–31,34,40,41] Extreme multielectron ionization of elemental and molecular clusters, e.g., Ar_n,[11,15,46–48] Xe_n,[12,22,24,34,43,44] $(H_2)_n$,[49] $(D_2)_n$,[28,50–53] $(H_2O)_n$,[42,54] $(D_2O)_n$,[35,42] $(CH_4)_n$,[38] $(CD_4)_n$,[28,38,55] and $(HI)_n$,[54,56,57] in ultraintense laser fields, leads to the production of highly charged ions. These involve the stripping of the valence electrons, or even of all the electrons from light first-row atoms, e.g., H^+ and D^+,[16,18,28,30,38,58] O^{q+} (q = 6–8),[18,35,59] and C^{q+} (q = 4–6),[20,28,32,38,42,59] as well as the production of highly charged heavy ions, e.g., Xe^{q+} (q = 3–36).[24,25,30,32,34,37,60,61] These unique inner/outer ionization processes and nanoplasma response manifest novel features of electron dynamics. This paper addresses extreme multielectron ionization and nanoplasma dynamics in elemental clusters.

2. METHODOLOGY

Cluster multielectron ionization, nanoplasma dynamics and response were explored by theoretical models[16,25,26,29,31,44,45,62–65] and by computer simulations.[13,18,29-32,34,37,40,53,58,63,65] Microscopic models for the cluster inner ionization level were based on the barrier suppression ionization (BSI) model.[30,64,65] An additional contribution to cluster inner ionization arises from electron impact ionization (EII) induced by the high-energy (50eV–1MeV) nanoplasma electrons.[29,33,37,65] The cluster outer ionization, which involves the (partial or complete) sweeping out of the nanoplasma electrons in the laser field, could be modeled by the entire cluster BSI model.[29,31,32] Molecular dynamics (MD) simulations[13,18,29-32,34,37,40,53,58,63,65] are useful for the confrontation with the predictions of microscopic or macroscopic models. For an $(A^{q+}(qe))_n$ cluster containing n A^{q+} ions and nq nanoplasma electrons, with N = n(q+1) particles, the computational workload increases as N^2. For $(Xe^{q+}(qe))_n$ clusters, which are of interest to us (with q = 3–36), such MD simulations are practical up to n = 3000 (i.e., $N = 10^4$–10^5). These computational methods will be used in the present work. Recent technical extensions of MD simulations were advanced,[41] based on a hierarchical tree code and cell models.[69] A promising approach based on scaling with the treatment of electron and nuclear miniclusters in clusters was advanced by us and will be reported elsewhere.[70]

We advanced[29,37,65] an MD simulation scheme for the high-energy electron dynamics and nuclear dynamics in a cluster interacting with an ultraintense laser field ($I_M = 10^{15}$–10^{20} W cm^{-2}). This scheme incorporated the coupling with the laser field, inner field effects of electrons and ions, screening and ionic fields by the electrons, and reactive EII. This scheme also includes magnetic field and relativistic effects, which are important in the highest intensity domain of $I_M = 10^{18}$–10^{20} W cm^{-2}. The laser electric field acting on the elemental or molecular cluster was taken as $F_\ell(t) = F_{\ell 0}(t)\cos(2\pi\nu t)$, where ν is the laser frequency and $F_{\ell 0}(t)$ is the pulse envelope function. We performed extensive MD simulations and analyses of high-energy electron dynamics and nuclear dynamics in Xe_n clusters (n = 2–2171) interacting with a Gaussian laser pulse $F_{\ell 0}(t) = F_M \exp[-2.773(t/\tau)^2]$. F_M is the electric field at the pulse peak, being related to the laser peak intensity by $F_M = 2.7448 \times 10^{-7}\ I_M^{1/2}$ (where F_M is given in eVÅ^{-1} and I_M in W cm^{-2}). For the laser parameters we used $\nu = 0.35$ fs^{-1} (photon energy 1.44 eV) and a pulse temporal width (FWHM) of τ = 10–100 fs. The laser pulse is defined in the time domain $t \geq -\infty$ and the peak of the laser pulse is attained at t = 0. An initially truncated laser pulse was used during the simulations, with the initial laser field (corresponding to the threshold of single electron/molecule ionization in the cluster) being located at the (negative) time $t = t_s$, which is laser-intensity- and pulse-width-dependent. The end of the pulse was characterized by the time $t = -t_s$.[37,65] Our simulations of electron dynamics elucidated the time dependence of inner ionization, the formation, persistence, and decay of the nanoplasma, and of outer ionization.

3. ELECTRON DYNAMICS AND GROSS FEATURES OF INNER/OUTER IONIZATION

A Xe_{2171} cluster coupled to a Gaussian laser pulse in the intensity range of $I_M = 10^{15}$–10^{19} W cm^{-2} with a pulse length of τ = 25 fs (Fig. 1) reveals the following general electron dynamics facets:

(1) The formation of an "electron cloud" inside or/and in the vicinity of the cluster.[30] This "electron cloud" is formed by inner ionization, which involves BSI and EII.[37,65]

(2) The nanoplasma consists of the electron cloud and of the positive Xe^{q+} ions. The nanoplasma responds to the laser field, which strips electrons from the cluster by outer ionization. Accordingly, the nanoplasma is positively charged.

(3) Spatial inhomogeneity and angular anisotropy of

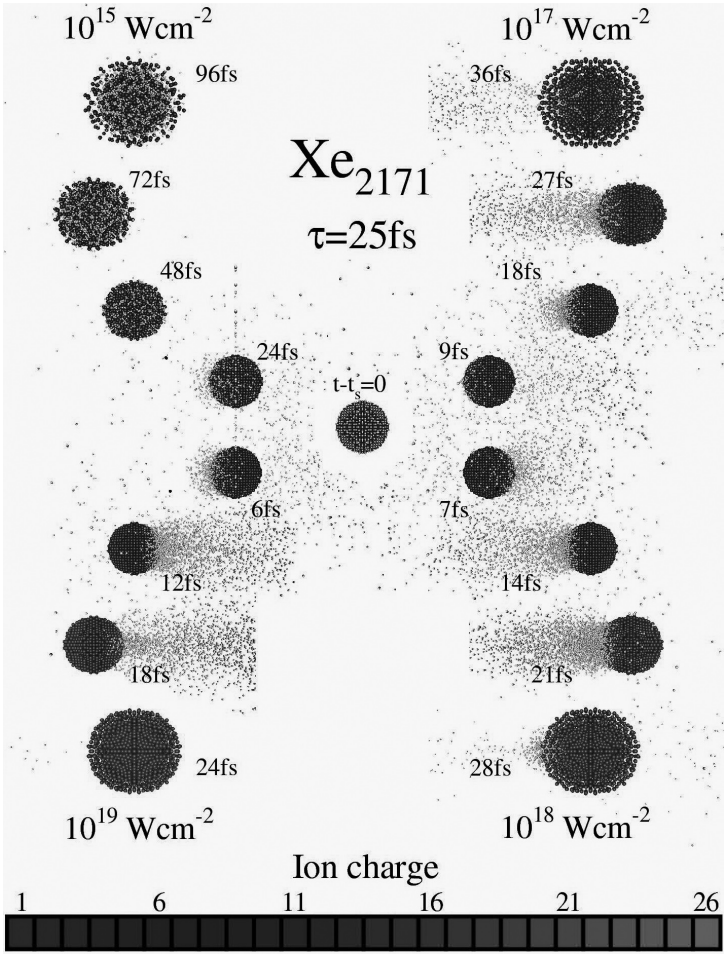

Fig. 1. Snapshots of the time-resolved ionization, nanoplasma charge distribution, and structures of Xe_{2171} clusters induced by Gaussian laser pulses with peak intensities $I_M = 10^{15}$ W cm^{-2}, 10^{17} W cm^{-2}, 10^{18} W cm^{-2}, and 10^{19} W cm^{-2} (marked on the 4 branches), and pulse width $\tau = 25$ fs. The initial configuration of the $(Xe^+(e))_{2171}$ cluster is located in the middle. The times (marked on the snapshots) represent $t–t_s$ values. The Xe atoms are color coded according to their charge: blue corresponds to the initial charge +1 and deep red to the maximum charge +26, which can be obtained for $I \geq 10^{18}$ W cm^{-2}. A map of the color coding of the charges is given at the bottom of the figure. The electrons are represented by light gray spheres. Color is seen online.

the nanoplasma. For $I_M = 10^{15}$ W cm^{-2} the electron cloud is nearly spatially isotropic, with the majority of the electrons being located within the cluster. For higher intensities of $I_M = 10^{18}$ W cm^{-2} and $I_M = 10^{19}$ W cm^{-2}, the electron angular distribution is spatially anisotropic, assuming a "sausage type" structure along the laser electric field direction.

(4) Attosecond–femtosecond response of the nanoplasma. At the intensities of $I_M = 10^{18}$–10^{19} W cm^{-2} the "sausage type" structure of the electron cloud oscillates along the electric field direction on the timescale ν^{-1} of the laser period, manifesting ultrafast electron dynamics.

(5) The outer ionization of the nanoplasma can be either partial (at intensities of 10^{15}–10^{16} W cm^{-2}) or complete (at highest intensities of 10^{18}–10^{20} W cm^{-2}).

(6) Persistent and transient nanoplasmas. At intensities of $I_M = 10^{15}$–10^{16} W cm^{-2}, where outer ionization is partial, a persistent nanoplasma on the timescale of $t–t_s > 100$ fs exists, while for higher intensities of $I_M = 10^{18}$–10^{19} W cm^{-2}, a transient nanoplasma is formed, being completely depleted on the timescale of $t–t_s \simeq 15$–25 fs.

(7) Sequential–parallel multielectron inner ionization, nanoplasma formation, and outer ionization are exhibited.

(8) Coulomb explosion, which is discussed elsewhere, occurs parallel and sequential with outer ioniza-

tion. The onset of Coulomb explosion of the multicharged cluster sets is prior to the completion of the outer ionization, with the appropriate timescale increasing with decreasing I_M. The cluster begins to expand significantly after ~60 fs at $I_M = 10^{15}$ W cm^{-2} and after ~25 fs at $I_M = 10^{18}$ W cm^{-2}.

We explored the dependence of the inner and the outer ionization levels, and of the electron dynamics (the response of the nanoplasma and the EII) on the cluster size and on the laser parameters (intensity and pulse length). Figure 2 presents the simulation results for the time dependence of the inner ionization, outer ionization, and nanoplasma population in Xe_n clusters (n = 459, 1061, and 2171) at intensities of $I_M = 10^{15}$ and 10^{18} W cm^{-2}. The total number of electrons N_{ii} produced by inner ionization is given by

$$N_{ii} = N_{BSI} + N_{imp} \quad (1)$$

where N_{BSI} is the total number of electrons produced by BSI and N_{imp} is the total number of electrons produced by EII. The inner ionization level per constituent atom is given by

$$n_{ii} = N_{ii}/n = n_{BSI} + n_{imp} \quad (2)$$

where the BSI level is $n_{BSI} = N_{BSI}/n$ and the EII level is $n_{imp} = N_{imp}/n$. The total number of electrons that were depleted by outer ionization is N_{oi} (with $N_{oi} \leq N_{ii}$), while the outer ionization level per constituent atom is given by

$$n_{oi} = N_{oi}/n \quad (3)$$

The total number of electrons in the nanoplasma is $N_p = N_{ii} - N_{oi}$ and the number $n_p = N_p/n$ of the electrons in the nanoplasma per constituent atom is given by

$$n_p = n_{ii} - n_{oi} \quad (4)$$

Figure 2 portrays the time dependence of the inner ionization level $n_{ii}(t)$ in the cluster size domain n = 459–2171 and for the laser intensities $I_M = 10^{15}$ and 10^{18} W cm^{-2}, with τ = 25 fs. $n_{ii}(t)$ reveals the gradual increase with increasing t, reaching saturation (at $I_M = 10^{18}$ W cm^{-2}) or near-saturation (at $I_M = 10^{15}$ W cm^{-2}) at the termination of the laser pulse ($t = -t_s$). This pattern of saturation/near-saturation of $n_{ii}(t)$ is cluster-size dependent. At $I_M = 10^{18}$ W cm^{-2}, the saturation of the outer ionization level, $n_{oi}(t)$, is exhibited at times longer than those for $n_{ii}(t)$ at the same intensity and cluster size, manifesting the sequential nature of the inner and outer ionization. At the lower intensity of $I_M = 10^{15}$ W cm^{-2} $n_{oi}(t)$ reaches saturation, while $n_{ii}(t)$ exhibits near-saturation due to the EII contribution.[37,65] The times characterizing the attainment of the saturation level of $n_{oi}(t)$ decrease with increasing I_M for all (fixed) values of n (Section 5). The limiting inner and outer ionization levels were characterized by $n_{ii}^L = n_{ii}(t_L)$ and $n_{oi}^L = n_{oi}(t_L)$ with t_L = 90fs. At fixed $I_M = 10^{15}$ and 10^{18} W cm^{-2}, n_{ii}^L increases with increasing n, due to the contribution of the inner field of the ions at these two intensities (Section 4). For outer ionization at $I_M = 10^{15}$ W cm^{-2}, n_{oi}^L decreases with decreasing the cluster size (to be discussed in Section 5), while at $I_M = 10^{18}$ W cm^{-2}, n_{oi}^L increases with increasing n. Concurrently, $n_{ii}^L > n_{oi}^L$ for $I_M = 10^{15}$ W cm^{-2}, while $n_{ii}^L = n_{oi}^L$ for $I_M = 10^{18}$ W cm^{-2}. These two qualitative differences between the inner/outer ionization levels at the two lower/higher intensity domains originate from the different nature of the nanoplasma, which is persistent at $I_M = 10^{15}$ W cm^{-2} and transient at $I_M = 10^{18}$ W cm^{-2}.[30,65]

The number of electrons in the nanoplasma $n_p(t)$, eq 4, saturates at long times for $I_M = 10^{15}$ W cm^{-2} (with $n_p^L = n_p(t_L)$), increasing with increasing n, as expected on the basis of the limiting outer ionization level in this intensity domain (Fig. 2). On the other hand, at $I_M = 10^{18}$ W cm^{-2}, the nanoplasma is completely depleted before the laser pulse reaches its peak, with the depletion process being more efficient with decreasing n, as manifested by the appearance of a maximum of $n_p(t)$ with a lower amplitude at lower values of n (Fig. 2). In conclusion, at the lower intensity range of $I_M = 10^{15}$ W cm^{-2}, "long-time" retention of the persistent nanoplasma (on the timescale of >100 fs) is exhibited, while in the highest intensity domain of $I_M \geq 10^{18}$ W cm^{-2} a transient nanoplasma (on the timescale of t_L for n = 459–2171) is produced.

4. MULTIELECTRON INNER IONIZATION LEVELS

The cluster inner ionization is driven by two processes:

(A) The BSI mechanism, which is induced by a composite field

$$\underset{\sim}{F} = \underset{\sim}{F}_\ell + \underset{\sim}{F}_I \quad (5)$$

where $\underset{\sim}{F}_\ell$ is the strong laser field, whose frequency satisfies two conditions, namely (i) it is considerably lower than the ionization potential for a single constituent atom and (ii) it is lower than the reciprocal barrier passage time, so that $\underset{\sim}{F}_\ell$ can be considered as a static field.[71] $\underset{\sim}{F}_I$ is the inner field, which is generated by all the other ions and by the electrons, acting on an ion (or atom) within the cluster. The potential for a q-fold ionized atom (or a neutral atom) formed by the nucleus with charge q and the composite static field $\underset{\sim}{F}$, eq 5, is characterized by a height U_b of the potential barrier

$$U_B = -2\left[eF\overline{B}(q+1)\right]^{1/2} \quad (6)$$

where $\overline{B}$ = 14.4 eV Å and $eF = e|\underset{\sim}{F}_\ell + \underset{\sim}{F}_I|$ is given in

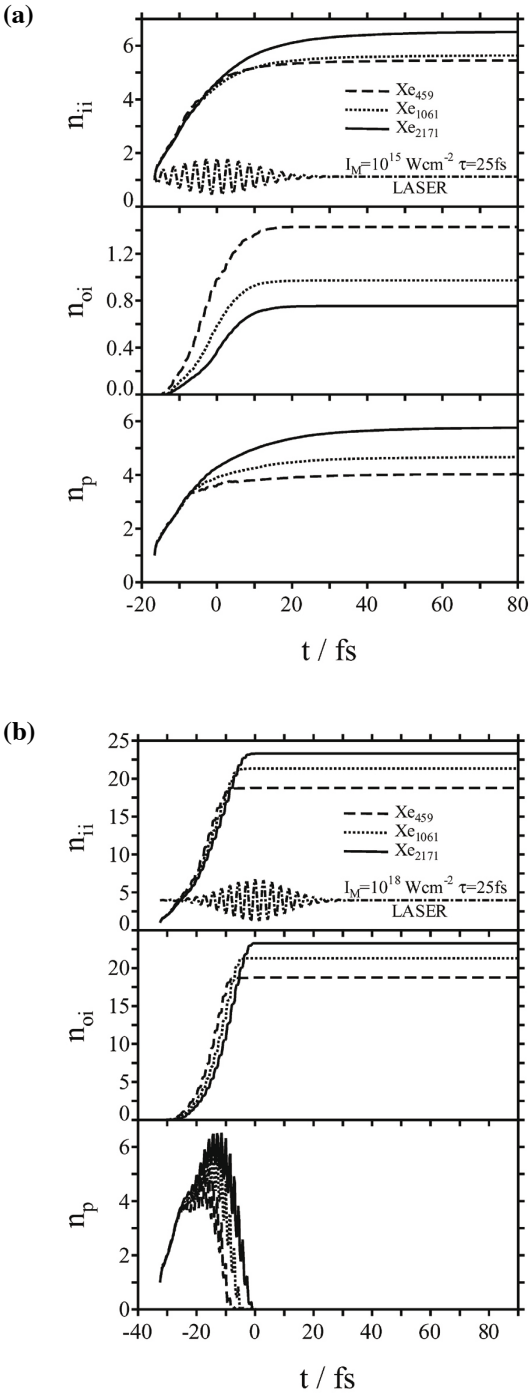

Fig. 2. The time-dependence of the inner ionization levels n_{ii}, the outer ionization levels n_{oi}, and the nanoplasma population $n_p = n_{ii}–n_{oi}$ for Xe_n clusters (n = 459, 1061, and 2171, as marked on the panels) for the intensities $I_M = 10^{15}$ W cm^{-2} (a) and $I_M = 10^{18}$ W cm^{-2} (b). The laser pulse width is $\tau = 25$ fs. The electric fields of the Gaussian laser pulses (–·–·–), expressed in arbitrary units for $t \geq t_s$, are represented on each upper panel, marked LASER.

units of eV Å^{-1}. The barrier is located at the distance

$$r_b = \left[\overline{B}(q+1)/eF\right]^{1/2} \quad (7)$$

from the ion center along the electric field direction. In the intensity range $I_M \geq 10^{15}$ W cm^{-2}, tunneling through the barrier is of minor importance. The BSI process for an ion (atom) in the cluster is realized with the barrier height, eq 6, being equal, with an opposite sign, to the ionization potential P_{q+1} of this ion. The threshold laser field for BSI is then given by

$$eF = P_{q+1}^2/4\overline{B}(q+1) \quad (8)$$

and the barrier distance, eq 7, is

$$r_b = 2\overline{B}(q+1)/P_{q+1} \quad (9)$$

The BSI contribution to inner ionization was evaluated from eq 8 with the threshold composite field, eq 5, and used as input data for the MD simulations of electron and nuclear dynamics. In this self-consistent scheme for cluster inner ionization there are two distinct contributions to the inner cluster field $\underset{\sim}{F}_I$:

(i) Electrostatic interactions with the ions, which can increase the compound field $\underset{\sim}{F}$ beyond the value of $\underset{\sim}{F}_\ell$, resulting in an inner field ignition effect on inner ionization.[29]

(ii) Electrostatic interactions with the nanoplasma electrons, which decrease the effective field below that of the "bare" ions, resulting in a screening effect on the inner field.[29,44]

(B) EII, which involves inelastic, reactive impact ionization of ions by the nanoplasma electrons. EII in Xe_n clusters was explored using experimental data for the energy dependence of ionization cross sections $\sigma_q(E)$ of Xe^{q+} ions (q = 1–10), which were fit by a three-parameter Lotz-type equation

$$\sigma_q(E) = a_q \frac{\ln(E/P_{q+1})}{EP_{q+1}}\left\{1 - b_q \exp\left[-c_q(E/P_{q+1})\right]\right\} \quad (10)$$

with the atomic ionization energy P_{q+1} and the adjustable parameters a_q, b_q, and c_q, which were obtained by fitting eq 10 to the experimental cross sections. Our work allowed for the proper parametrization of the EII cross sections, leading to reliable information on the EII ionization levels and their relative contribution to inner ionization and to the nanoplasma populations. At the lower intensity domain of $I_M = 10^{15}$–10^{16} W cm^{-2}, the EII contribution to the inner ionization yield is substantial ($\simeq$50% for Xe_{2171} at $\tau = 25$ fs), increases with increasing the cluster size, and manifests a marked increase with increasing the pulse length. The EII yield and the EII level enhancement markedly decrease with increasing the laser intensity, being small for $I_M \geq 10^{18}$ W cm^{-2}. EII

reactive dynamics is important in the lower intensity domain where the persistent nanoplasma prevails (Section 3), being of minor importance in the higher intensity range where the nanoplasma is transient.

Multielectron ionization of Xe_n clusters containing many-electron heavy atoms qualitatively differs from that of molecular clusters containing "light" first-row atoms, e.g., $(H_2)_n$, $(D_2)_n$,[28,40,49–53] $(CH_4)_n$, and $(CD_4)_n$.[28,38,55] The difference stems from the dependence of the ionization level of Xe_n clusters on the laser intensity and cluster size dependence. In clusters consisting of light atoms, complete inner/outer ionization with the formation of nuclei can be achieved at accessible laser intensities, e.g., the production of $(D^+)_n$ at $I_M = 8 \times 10^{14}$ W cm^{-2} or of $(C^{6+}(D_4^+)_n)$ at $I_M = 10^{19}$ W cm^{-2}.[29] On the other hand, for Xe_n clusters there is no saturation limit for the increase of the Xe ion ionization level by increasing the laser intensity in the experimentally accessible domain of $I_M < 10^{21}$ W cm^{-2}. The cluster size dependence of the ionization level at different intensities, due to ignition and screening effects, were also analyzed in detail.[65] In Fig. 3 we present the laser intensity dependence (for Gaussian pulses with $\tau = 25$ fs in the range $I_M = 10^{15}$–10^{20} W cm^{-2}) and cluster size dependence (in the range of n = 55–2171) of the average ionization level $q_{av} = n_{ii}^L$ of Xe^{q+} ions produced by inner/outer ionization of Xe_n clusters. The most dramatic effect is the marked increase of q_{av} with increasing I_M at a fixed cluster size. A rough correlation is exhibited for the intensity-dependent ionization levels with "magic numbers" $q_{av} = 8,18,26,36$ in multielectron ionization, which involve the ionization of entire closed electronic shells of the constituents.[65] Such "magic numbers" (marked in Fig. 3) are exhibited when the BSI mechanism dominates, being manifested for small ($n \leq 55$) clusters over the intensity range of $I_M = 10^{16}$–10^{18} W cm^{-2} and for the entire size domain over the intensity range of $I_M = 10^{15}$–10^{20} W cm^{-2} (Fig. 3). The rather complex cluster size dependence of q_{av} at a fixed intensity manifests an increase with increasing n at $I_M = 10^{17}$ W cm^{-2} (n = 55–459) and at $I_M = 10^{18}$ W cm^{-2} (n = 55–2171), which is due to ignition effects and a decrease with decreasing n at $I_M = 10^{17}$ W cm^{-2} (n = 459–2171) and at $I_M = 10^{16}$ W cm^{-2} (n = 55–2171), which is due to screening effects. "Magic numbers" in cluster multielectron ionization are observed in the cluster size domain where laser-induced BSI dominates over ignition, screening, and EII. The "magic numbers" are $q_{av} = 8$ at $I_M = 10^{16}$ W cm^{-2} for n = 2–55, corresponding to the ionization of the $5s^25p^6$ shells, $q_{av} = 18$ at $I_M = 10^{18}$ W cm^{-2} for n = 2–135, corresponding to the ionization of the $4d^{10}5s^25p^6$ shells, $q_{av} = 26$ at $I_M = 10^{19}$ W cm^{-2} for n = 55–2171, corresponding to the ionization of the $4s^24p^64d^{10}5s^25p^6$ shells, and $q_{av} = 36$ at $I_M = 10^{20}$ W cm^{-2} for n = 55–2171, corresponding to the ionization of the $3d^{10}4s^24p^64d^{10}5s^25p^6$ shells.

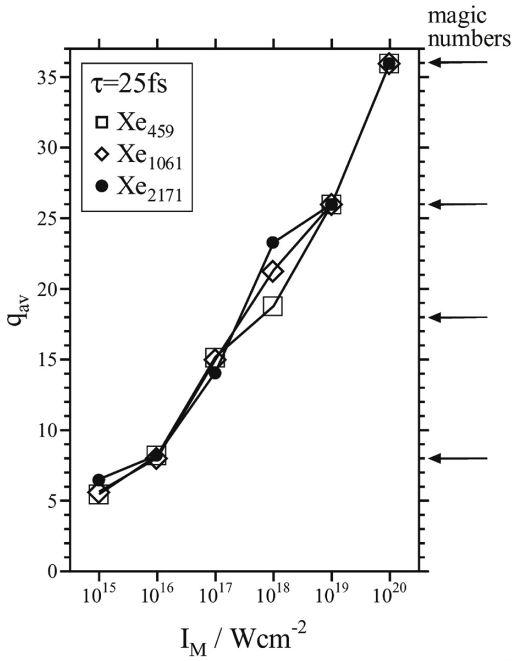

Fig. 3. Laser intensity dependence of inner ionization levels (expressed by the average charge $q_{av} = n_{ii}^L$ of the $\{Xe^{q+}\}_n$ ions) of Xe_n clusters (n = 459–2171) over the intensity range $I_M = 10^{15}$–10^{20} W cm^{-2} (marked on the curves) with a laser pulse width of $\tau = 25$ fs. The horizontal arrows (marked atomic limit) represent the "magic numbers" for the ionization of entire closed electronic shells.

5. OUTER IONIZATION

The nanoplasma is formed from the unbound electrons, which are confined to the cluster and to its vicinity, and from the ions. The life story of the nanoplasma is portrayed in Fig. 1 for Xe_{2171} clusters. These snapshots portray the formation of the nanoplasma, its response to the laser field, followed by its complete depletion at $I_M = 10^{18}$ W cm^{-2} or its partial depletion at $I_M = 10^{15}$ W cm^{-2} (Fig. 1). The time-dependent nanoplasma population is characterized by the number $n_p(t)$, eq 4, of nanoplasma electrons (per atomic constituent). The number of depleted electrons (per constituent) for outer ionization exhibits a gradual increase and long-time saturation (Fig. 4). At long times, after the termination of the laser pulse, the population is persistent at lower intensities of $I_M = 10^{15}$–10^{16} W cm^{-2}, exhibiting only partial depletion (Fig. 4). The long-time population n_p^L of the nanoplasma

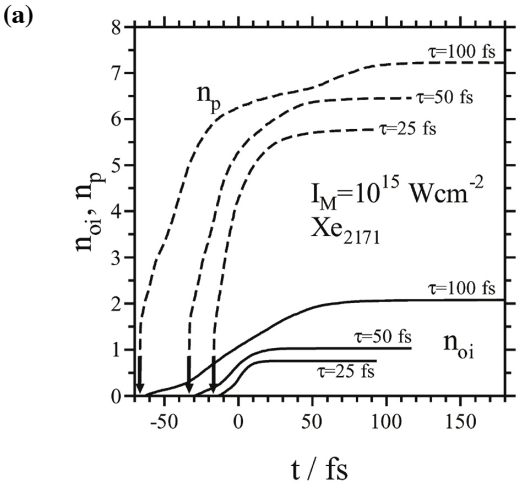

Fig. 4. The time-dependent distribution of the ionic charges n(q) of $(Xe^{q+})_n$ ions at times $t–t_s$ = 5–125 fs (with the times marked on the panels) created by the inner ionization of Xe_{2171} clusters with a Gaussian laser pulse (τ = 25 fs) at intensities of $I_M = 10^{15}$ W cm^{-2}.

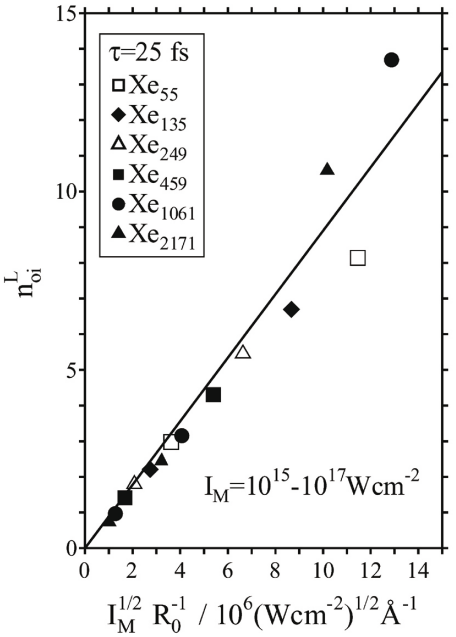

Fig. 5. The cluster size and laser intensity dependence of the long-time EII level n^L_{imp} for Xe_n (n = 55–2171) clusters in the intensity range $I_M = 10^{15}$–10^{20} W cm^{-2} (τ = 25 fs).

manifests a marked increase with increasing the pulse length.

Cluster outer ionization manifests the nanoplasma response to the laser field, due to barrier suppression of the entire cluster and due to quasiresonance effects. The outer ionization removes all, or part, of the nanoplasma electrons by the laser field. We described outer ionization in terms of a cluster barrier suppression ionization (CBSI) model, which involves the balancing between the cluster exterior Coulomb potential and the laser field potential at the cluster boundary. The long-time outer ionization level was expressed in the form

$$n^L_{oi} = F_M \gamma \xi^2 / \left(\frac{4\pi\sqrt{2}}{3}\right) \overline{B} \rho_{mol} R_0 \qquad (11)$$

where F_M is the laser electric field for peak intensity I_M, $\rho_{mol} = 3n/4\pi R_0^3$ is the initial atomic/molecular constituent density expressed in terms of the initial cluster radius,

$$\xi = R(t)/R_0 \qquad (12)$$

is the cluster expansion parameter due to Coulomb explosion, and $\gamma \simeq 4$ is a numerical correction factor, accounting for deviations from the electrostatic model. This result is applicable for the intensity range and cluster size domain where a persistent nanoplasma prevails, i.e., $n^L_{ii} > n^L_{oi}$. The use of eq 11 gives

$$n^L_{oi} = A I_M^{1/2} / R_0 \qquad (13)$$

where

$$A = 2.745 \cdot 10^{-7} \gamma \xi^2 / \left(4\pi\sqrt{2}/3\right) \overline{B} \rho_{mol} \qquad (14)$$

In eqs 13 and 14, I_M is presented in W cm^{-2}, R_0 in Å, ρ_A in Å^{-3}, and $\overline{B}$ = 14.4 eV Å. The most striking prediction of the CBSI model, which is confirmed by our simulation data, is the linear dependence of n^L_{oi} on $I_M^{1/2}$ over a broad laser intensity and cluster size range (at fixed τ), where the persistent nanoplasma exists. A typical example is portrayed in Fig. 5 for τ = 25 fs with n = 55–2171, and $I_M = 10^{15}$–10^{17} W cm^{-2}. From the dependence of the compound parameter $\gamma^{1/2}\xi$ on τ, we inferred that the outer ionization level for Xe_n clusters is[65]

$$n^L_{oi} = 1.06 \cdot 10^{-7} \tau^{0.64} I_M^{1/2} / R_0 \qquad (15)$$

where R_0 is given in Å, I_M in W cm^{-2}, and τ in fs. An identical function of the form $n^L_{oi} \propto \tau^{0.62} I_M^{1/2}/R_0$ was previously obtained for outer ionization of $(D_2)_n$ clusters,[72] pointing towards the generality of the electrostatic CBSI model. It is also gratifying that the relation between the electron outer ionization levels and the expansion parameter, ξ, eq 12 provides information on nuclear Coulomb explosion dynamics.

6. CONCLUDING REMARKS

We explored cluster–ultraintense laser interactions that drive extreme multielectron ionization, in conjunction

with attosecond–femtosecond electron dynamics of the resulting nanoplasma in elemental Xe_n clusters. The Rabi frequency for the interaction of an ultraintense laser ($I_M = 10^{18}$ W cm^{-2}), with an atom or molecule with a transition moment of 1–5 Debye, falls in the range of 2–10 k eV. Such high values of the Rabi frequency signal the breakdown of the perturbative quantum electro-dynamics approach for the ultraintense laser–atom/molecule interaction. A nonperturbative treatment of cluster ionization mechanisms, the extreme multielectron ionization levels, and the characteristics and response of the nanoplasma, is imperative in this ultrahigh intensity domain, being based on theoretical models and computational molecular dynamics simulations. The microscopic approach, which rests on the three sequential–parallel processes of inner ionization, nanoplasma formation and response, and outer ionization, provided a complete description of cluster extreme multielectron ionization and electron dynamics. In this complex system where phase coherence is eroded, these three processes are separable. The physical reality is complex, but manageable, being amenable to a proper analysis over broad cluster size, laser intensity, and laser pulse width domains.

The nanoplasma consists of an "electron cloud" within the cluster or in its vicinity and of positive ions within the nuclear framework of the clusters. Of considerable interest is the production of a persistent nanoplasma in Xe_n clusters (n = 459–2171) at lower intensities (and larger cluster sizes) and a transient nanoplasma at higher laser intensities (and smaller cluster sizes).

The analysis of the (time-resolved) inner ionization levels of Xe_n clusters manifests some unique features. The laser intensity-dependent ionization levels of Xe_n clusters, with the dramatic enhancement of q_{av} with increasing I_M, originate from the laser field contribution to the BSI. This enhancement is characteristic for multielectron partial inner ionization of heavy atoms, with no production of bare nuclei in the currently available laser intensity domain ($I_M \leq 10^{21}$ W cm^{-2}). On the other hand, for $(H_2)_n$ and $(D_2)_n$ clusters, complete ionization can be achieved at $I_M \simeq 8 \times 10^{14}$ W cm^{-2}, which is below the lowest limits of the intensity range used herein. For first-row molecular heteroclusters consisting of light atoms, e.g., $(CA_4)_n$, $(A_2O)_n$ (A = H, D), complete multielectron ionization, with the production of H^+, D^+, C^{6+}, and O^{8+} nuclei, can be realized. We also found that EII is important for clusters of heavy multielectron atoms or molecules, e.g., Xe_n, where the corresponding cross sections are large.[37] The largest EII yields are exhibited at $I_M = 10^{15}$–10^{16} W cm^{-2}, where the persistent nanoplasma prevails (for n > 55). Significantly, in the persistent nanoplasma domain (at $I_M = 10^{15}$ –10^{16} W cm^{-2}), the EII yields and the values of q_{av} and q_{max} manifest a marked increase with increasing the laser pulse length (Fig. 4). EII dynamics opens avenues for the control of reaction ionization products from clusters in ultraintense laser fields.

The gross features of the outer ionization process were adequately described by the electrostatic CBSI model, which predicts the linear dependence of n_{oi}^{L} vs. $I_M^{1/2}/R_0$, being in good agreement with simulation results, and providing new information on the relative values of the cluster expansion parameter ξ and its pulse length dependence. Further exploration of the fitting parameter γ in the electrostatic model, eqs 12 and 14, which arises from the finite energy of the nanoplasma and incomplete inner/outer ionization at the laser peak, is called for. In spite of this success of the electrostatic model, the complete description of outer ionization in terms of quasiresonance nonlinear effects in nanoplasma–laser interactions is still lacking. Some recent numerical simulations pertain to this issue.[29]

Acknowledgments. This research was supported by the Deutsche Forschungsgemeinschaft (DFG) SFB 450 on "Analysis and Control of Ultrafast Photoinduced Reactions" and by the James Franck Binational German-Israeli Program in Laser-Matter Interaction.

REFERENCES AND NOTES

(1) Perry, M.D.; Mourou, G.A. *Science* **1994**, *264*, 917.
(2) Mourou, G.A.; Barty, C.P.J.; Perry, M.D. *Phys. Today* **1998**, *51*, 22.
(3) Zewail, A.H. *Femtochemistry: Ultrafast Dynamics of the Chemical Bond*; World Scientific: Singapore, 1994.
(4) Manz, J.; Wöste, W., Eds.: *Femtosecond Chemistry*; VCH: Weinheim, 1995.
(5) Chergui, M., Ed. *Femtochemistry: Ultrafast Chemical and Physical Processes in Molecular Systems*; World Scientific: Singapore, 1996.
(6) Söndstrom, V., Ed.: *Femtochemistry and Femtobiology*; Nobel Symposium 101, Imperial College Press: London, 1997.
(7) Corkum, P.B. *Phys. Rev. Lett.* **1993**, *71*, 1994.
(8) Jortner, J. *Proc. R. Soc. London, Series A* **1998**, *356*, 477.
(9) Krausz, F. *Optics and Photonic News*, May issue **2002**, p 62.
(10) Bahrdway, V.E.; Corkum, P.B.; Rymer, D.M. *Phys. Rev. Lett.* **2005**, *93*, 5400.
(11) Ditmire, T.; Donnely, T.; Rubenchik, A.M.; Falcone, R.W.; Perry, M.D. *Phys. Rev. A* **1996**, *53*, 3379.
(12) Ditmire, T.; Tisch, J.W.G.; Springate, E.; Mason, M.B.; Hay, N.; Smith, R.A.; Marangos, J.; Hutchinson, M.H.R. *Nature* **1997**, *386*, 54.
(13) Ditmire, T. *Phys. Rev. A* **1998**, *57*, R4094.
(14) Ishikava, K.; Blenski, T. *Phys. Rev. A* **2000**, *62*, 063204.

(15) Liu, J.; Li, R.; Zhu, P.; Xu, Zh.; Liu, J. *Phys. Rev. A* **2001**, *64*, 033426.
(16) Parks, P.B.; Cowan, T.E.; Stephens, R.B.; Campbell, E.M. *Phys. Rev. A* **2001**, *63*, 063203.
(17) Krainov, V.P.; Roshchupkin, A.S. *J. Phys. B* **2001**, *34*, L297.
(18) Last, I.; Jortner, J. *Phys. Rev. A* **2001**, *64*, 063201.
(19) Krainov, V.P.; Smirnov, M.B. *Phys. Rep.* **2002**, *370*, 237.
(20) Card, D.A.; Wisniewski, E.S.; Folmer, D.E.; Castleman, A.W.Jr. *J. Chem. Phys.* **2002**, *116*, 3354.
(21) Saalmann, U.; Rost, J.M. *Phys. Rev. Lett.* **2002**, *89*, 143401.
(22) Lezius, M.; Blanchet, V.; Ivanov, M.Yu.; Stolow, A. *J. Chem. Phys.* **2002**, *117*, 1575.
(23) Bauer, D.; Macchi, A. *Phys. Rev. A* **2003**, *68*, 033201.
(24) Schulz, J.; Wabnitz, H.; Laarmann, T.; Gürtler, S.; Laasch, W.; Swiderski, A.; Möller, Th.; de Castro, A.A.B. *Nucl. Instrum. Methods Phys. A* **2003**, *507*, 572.
(25) Siedschlag, Ch.; Rost, J.-M. *Phys. Rev. A* **2003**, *67*, 13404.
(26) (a) Siedschlag, Ch.; Rost, J.-M. *Phys. Rev. Lett.* **2004**, *93*, 043402. (b) Siedschlag, Ch.; Rost, J.-M. *Phys. Rev. A* **2004**, *71*, 031401.
(27) Laarman, T.; De Castro, A.R.B.; Gürtler, P.; Laasch, W.; Schulz, J.; Wabnitz, H.; Möller, T. *Phys. Rev. Lett.* **2004**, *92*, 143401.
(28) Madison, K.W.; Patel, P.K.; Price, D.; Edens, A.; Allen, M.; Cowan, T.E.; Zweiback, J.; Ditmire, T. *Phys. Plasmas* **2004**, *11*, 270.
(29) Last, I.; Jortner, J. *J. Chem. Phys.* **2004**, *120*, 1336.
(30) Last, I.; Jortner, J. *J. Chem. Phys.* **2004**, *120*, 1348.
(31) Last, I.; Jortner, J. *J. Chem. Phys.* **2004**, *121*, 3030.
(32) Last, I.; Jortner, J. *J. Chem. Phys.* **2004**, *121*, 8329.
(33) Zamith, S.; Martchenko, T.; Ni, Y.; Aseyev, S.A.; Muller, H.G.; Vrakking, H.J.J. *Phys. Rev. A* **2004**, *70*, 011201(R).
(34) Martchenko, T.; Siedschlag, Ch.; Zamith, S.; Muller, H.G.; Vrakking, M.J.J. *Phys. Rev. A* **2005**, *72*, 053202.
(35) Ter-Avetisyan, S.; Schnürer, M.; Hilscher, D.; Jahnke, U.; Bush, S.; Nickles, P.V.; Sandner, W. *Phys. Plasmas* **2005**, *12*, 012702.
(36) Niu, D.; Li, H.; Liang, F.; Wen, L.; Luo, X. *J. Chem. Phys.* **2005**, *122*, 151103.
(37) Heidenreich, A.; Last, I.; Jortner, J. *Eur. Phys. J. D* **2005**, *35*, 567.
(38) Hokenberger, M.; Symes, D.R.; Madison, K.W.; Sumeruk, A.; Dyer, G.; Edens, A.; Grigsby, W.; Hays, G.; Teichmann, M.; Ditmire, T. *Phys. Rev. Lett.* **2005**, *95*, 195003.
(39) Ter-Avetisyan, S.; Schnürer, M.; Nickles, P.V.; Kalashnikov, M.; Risse, E.; Sokollik, T.; Sandner, W.; Andreev, A.; Tikhonchuk, V. *Phys. Rev. Lett.* **2006**, *96*, 145006.
(40) Last, I.; Jortner, J. *Phys. Rev. A* **2006**, *73*, 013202.
(41) Siedschlag, Ch.; Rost, J.M. *Phys. Rev. Lett.* **2002**, *89*, 173401.
(42) Kumarappan, V.; Krishnamurthy, M.; Mathur, D. *Phys. Rev. A* **2003**, *67*, 063207.
(43) Springate, E.; Aseyev, S.A.; Zamith, S.; Vrakking, M. J. J. *Phys. Rev. A* **2003**, *68*, 053201.
(44) Rusek, M.; Orlowski, A. *Phys. Rev. A* **2005**, *71*, 043202.
(45) Ter-Avetisyan, S.; Schnürer, M.; Hilscher, D.; Jahnke, U.; Busch, S.; Nickles, P.V.; Sandner, W. *Phys. Plasmas* **2005**, *12*, 012702.
(46) Krishnamurthy, M.; Mathur, D.; Kumarappan, V. *Phys. Rev. A* **2004**, *69*, 033202.
(47) Liu, J.; Wang, Ch.; Liu, B.; Shuai, B.; Wang, W.; Cai, Y.; Li, H.; Ni, G.; Li, R.; Xu, Z. *Phys. Rev. A* **2006**, *73*, 033201.
(48) Hirokane, M.; Shimizu, S.; Hashida, M.; Okada, S.; Okihara, S.; Sato, F.; Iida, T.; Sakabe, S. *Phys. Rev. A* **2004**, *69*, 063201.
(49) Sakabe, S.; Shimizu, S.; Hashida, M.; Sato, F.; Tsuyukushi, T.; Nishihara, K.; Okihara, S.; Kagawa, T.; Izawa, Y.; Imasaki, K.; Lida, T. *Phys. Rev. A* **2004**, *69*, 023203.
(50) Zweiback, J.; Cowan, T.E.; Smith, R.A.; Hurtlay, J.H.; Howell, R.; Steinke, C.A.; Hays, G.; Wharton, K.B.; Krane, J.K.; Ditmire, T. *Phys. Rev. Lett.* **2000**, *85*, 3640.
(51) Zweiback, J.; Cowan, T.E.; Hartley, J.M.; Howell, R.; Wharton, K.B.; Crane, J.K.; Yanovski, V.P.; Hays, G.; Smith, R.A.; Ditmire, T. *Phys. Plasmas* **2002** *9*, 3108.
(52) Madison, K.W.; Patel, P.K.; Allen, M.; Price, D.; Fitzpatrick, R.; Ditmire, T. *Phys. Rev. A* **2004**, *70*, 053201.
(53) Isla, M.; Alonso, J.A. *Phys. Rev. A* **2005**, *72*, 023201.
(54) Dermota, T.E.; Hydutsky, D.P.; Bianco, N.J.; Castleman, A.W.Jr. *J. Chem. Phys.* **2005**, *123*, 214308.
(55) Grillon, G.; Balcou, Ph.; Chambaret, J.-P.; Hulin, D.; Martino, J.; Moustaizis, S.; Notebaert, L.; Pittman, M.; Pussieux, Th.; Rousse, A.; Rousseau, J.-Ph.; Sebban, S.; Sublemontier, O.; Schmidt, M. *Phys. Rev. Lett.* **2002**, *89*, 065005.
(56) Purnell, J.; Snyder, E.M.; Wei, S.; Castleman, A.W.Jr. *Chem. Phys. Lett.* **1994**, *229*, 333.
(57) Tisch, J.W.G.; Hay, N.; Springate, E.; Gumbrell, E.T.; Hutchinson, M.H.R.; Marangos, J.P. *Phys. Rev. A* **1999**, *60*, 3076.
(58) Eloy, M.; Azambuja, R.; Mendonca, T.M.; Bingham, R. *Phys. Plasmas* **2001**, *8*, 1084.
(59) Toma, E.S.; Muller, H.G. *Phys. Rev. A* **2002**, *66*, 013204.
(60) Fukuda, Y.; Yamakawa, K.; Akahane, Y.; Aoyama, M.; Inoue, N.; Ueda, H.; Kishimoto, Y. *Phys. Rev. A* **2003**, *67*, 061201 (R).
(61) Siedschlag, Ch.; Rost, J.M. *Phys. Rev. A* **2005**, *71*, 031401 (R).
(62) Mijoule, V.; Lewis, L.J.; Meunier, M. *Phys. Rev. A* **2006**, *73*, 033203.
(63) Jungreuthmayer, Ch.; Geissler, M.; Zanghellini, J.; Brabec, T. *Phys. Rev. Lett.* **2004**, *92*, 133401.
(64) Augst, S.; Strickland, D.; Meyerhofer, D.D.; Chin, S.L.; Eberly, J. *Phys. Rev. Lett.* **1989**, *63*, 2212.

(65) Heidenreich, A.; Last, I.; Jortner, J. *J. Chem. Phys.* **2007**, *127*, 074305-1.
(66) Fomichev, S.V.; Popruzhenko, S.V.; Zaretsky, D.F.; Becker, W. *J. Phys. B* **2003**, *36*, 3817.
(67) Mulser, P.; Kanapathipillai, M.; Hoffmann, D.H.H. *Phys. Rev. Lett.* **2005**, *95*, 103401.
(68) Kundu, M.; Bauer, D. *Phys. Rev. Lett.* **2006**, *96*, 123401.
(69) (a) Barnes, J.E.; Hut, P. *Nature* **1986**, *324*, 446. (b) Pfalzner, S.; Gibbon, P. *Many-Body Tree Methods in Physics*; Cambridge University Press: Cambridge, U.K., 1996.
(70) Heidenreich, A.; Last, I.; Jortner, J. *Eur. Phys. J.* **2008**, *46*, 195.
(71) Keldysh, L. V. *Sov. Phys. JETP* **1965**, *20*, 1307.
(72) Last, I.; Jortner, J. *Phys. Rev. A* **2006**, *73*, 063201.